The controlled-drift detector

A. Castoldi[a,*], E. Gatti[a], C. Guazzoni[a], A. Longoni[a], P. Rehak[b], L. Strüder[c]

[a]*Politecnico di Milano, P.za L. da Vinci 32, 20133 Milano, Italy*
[b]*Brookhaven National Laboratory, Upton, NY 11973, USA*
[c]*MPI Halbleiterlabor, Otto-Hahn-Ring 6, D-81739 München, Germany*

Abstract

A new position-sensing X-ray detector is presented. The novel device is called Controlled-Drift Detector (CDD). The detector is fully depleted and is operated by switching between integration and drift modes. The relevant details of the detector design are discussed. A complete experimental characterization of the fast readout of the integrated signal charges achievable with static drift fields in the range 100–400 V/cm has been carried out. Preliminary measurements to evaluate the charge-handling capacity are also shown. The CDD can provide unambiguous two-dimensional position measurement, high-resolution X-ray spectroscopy and time resolution below 1 ms.

1. Introduction

A new position-sensing X-ray detector, called Controlled-Drift Detector (CDD), was recently proposed and the first experimental evidence of its working principle was reported [1,2]. The device is fully depleted and operates by switching between integration and drift modes. The basic idea of the CDD is to generate columns of equally spaced potential wells for the electrons by superposing a periodic perturbation of sufficient amplitude to a linear drift potential. During the integration mode the signal electrons are stored within these wells. The removal of this perturbation in an externally controlled way restores the linear drift potential that sweeps the electrons towards the collecting anodes. The drift field can be high enough to provide drift velocities comparable to the ones measured in silicon drift detectors [3].

The time between the removal of the potential barriers and the arrival of the signal electrons at the collecting anodes gives the position of the irradiated pixel along the drift direction. The second coordinate is obtained providing a separate readout anode for each pixel column. The collected signal charge measures the energy of the X-ray with spectroscopic resolution.

Different design solutions have been proposed to implement the concept of the CDD [1], depending

on the way the periodic potential perturbation is generated inside the detector volume (e.g. by a suitable biasing scheme of the field electrodes or by a doping pattern). Channel-stop implants provide permanent potential barriers that suppress charge cloud broadening in the direction transversal to the drift during the whole integrate-drift cycle.

Full depletion of the detector wafer allows for high X-ray efficiency at the higher-energy photons ($>50\%$ efficiency up to 20 keV photons for a 300 μm thick wafer), for small output capacitance and for back illumination. The entrance window on the back side can be realized with a continuous pn junction that allows to extend the low-energy response down to 150 eV by means of a careful optimization of the doping profile [4].

A similar readout mechanism, based on resistive gate electrodes, was developed by Philips Research Laboratories in an image sensor for visible-light applications [5]. In that device the electron packet was stored in a MOS cell and was transferred to a shallow channel parallel to the storage column for the transport to the output electrode. The CDD is based on reverse-biased pn junctions instead of MOS structures and both integration and transport of the signal electrons take place several microns deep in the fully depleted high-purity bulk. Higher drift velocities are expected, approaching the product of the bulk mobility of the carriers times the applied drift field.

In this paper we present an experimental characterization of the main operating features of one prototype of the CDD. The integration-drift cycle has been tested as a function of the drift field in the range 100–400 V/cm, the energy resolution achievable with the on-chip electronics has been measured and a preliminary estimate of the charge handling capacity has been obtained.

2. Detector design

Prototypes of the Controlled Drift Detector were produced at MPI Halbleiterlabor in Munich on the same wafers as the fully depleted pn-Charge Coupled Devices. The material and all technological steps are thus identical to the pn-Charge Coupled Device production [6]. The available
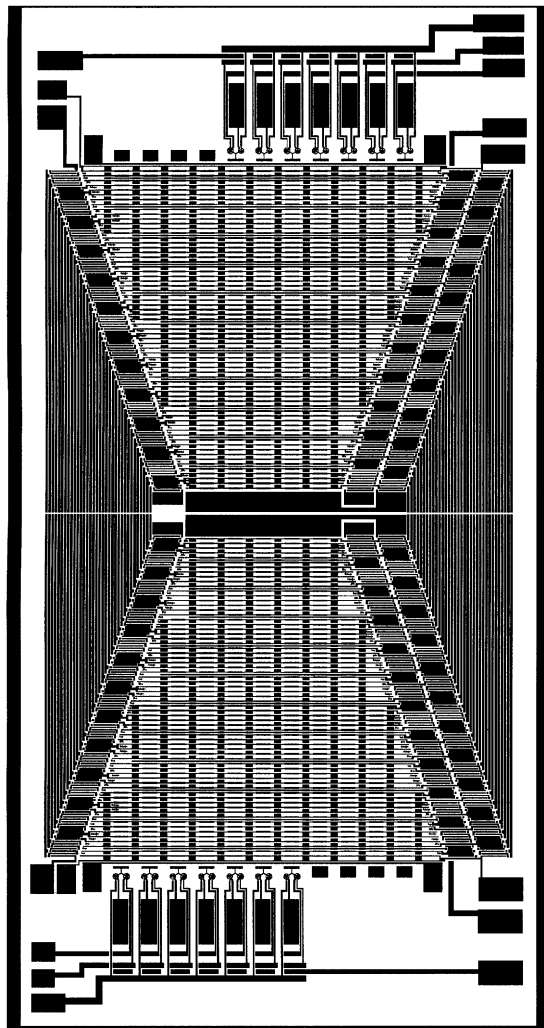

Fig. 1. Metalization mask of the front side of the Controlled-Drift Detector.

starting material was a 280 μm thick n-type 3 kΩ cm substrate on which an n-type 50 Ω cm epitaxial layer 15 μm thick is grown. Fig. 1 shows the metalization mask of the active and guard area of the detector's front side. This CDD prototype is characterized by two different biasing schemes of the field strips, one for the integration phase and one for the drift phase. During the drift phase the drift field acting on the electrons is obtained by biasing the field strips of the front side of the CDD at linearly increasing negative potentials moving

farther from the collecting anode, like in a silicon drift detector. During the integration phase some of the field strips are biased at higher and lower potentials with respect to the drift biasing scheme in order to superpose a periodic perturbation able to block the drift to the linear potential.

To be more quantitative, let us idealize the potential perturbation at the front surface ($z = 0$) with the sine wave $\Delta V_p \sin((2\pi/P_y)y)$, where y is the drift direction and P_y is the period, corresponding to the pixel length. The perturbation in the detector volume is given by

$$\Delta V_p \, \sin\left(\frac{2\pi}{P_y} \, y\right) \exp\left(-\frac{2\pi}{P_y} \, z\right) \quad (1)$$

where $z \ll d$ and $2\pi d/P_y \gg 1$ is assumed, d being the total detector thickness. At the depth where the potential minimum for the electrons is located a barrier in the drift direction is obtained only if the perturbation amplitude $\Delta V_p \exp(-(2\pi/P_y)z)$ is greater than the threshold value $(E_d P_y/2\pi)$ set by the drift field E_d. This criterion is the guideline for the design of the detector. As initial specifications of the design we assumed a pixel length $P_y = 180$ μm and operating fields in the range 100–400 V/cm. From the sinusoidal approximation we expect that values of ΔV_p of the order of 2 V are able to block the drift of the signal electrons down to a depth of about $z = 12$ μm.

For a given pixel length P_y a compromise must be made in the choice of the pitch of the field strips. A long pitch results in a poor approximation of the sinusoidal shape of the surface perturbation leading to a greater effect of higher-order harmonics. A long pitch has also a negative effect on the uniformity of the drift field during readout, leading to a more significant reduction of the electron velocity. On the other hand a short pitch leads to small size structures, high number of metal interconnections per pixel and is eventually limited by the yield of the lithographic process. The chosen pitch of 30 μm (25 μm p^+ implant, 5 μm oxide) assures acceptable non uniformity of the drift field during the readout phase and allows six strips to form the sinusoidal-like perturbation during the integration phase. Deviations from the sinusoidal shape are in this case mainly due to the sixth-order

harmonic that, at the depth of 12 μm, is already a factor 8 smaller than the fundamental one.

Figs. 2a and b show the contour lines of the potential energy in a detector cross section in the middle of a pixel column during the integration phase and during the drift phase obtained by a Poisson solver assuming full depletion of the bulk. The drift field is 300 V/cm, equivalent to a constant potential difference of 0.9 V between contiguous strips during the drift phase, while the amplitude of the applied voltage change is $\Delta V_{sw} = 2$ V. In Fig. 2a the integration well located at a depth $z \cong 12$ μm is clearly visible. The potential barrier from the integration minimum to the saddle point limits the maximum storable charge in the pixel. In conditions of vanishing signal charge, Fig. 2a shows that a potential barrier of about 920 mV is obtained. For increasing signal charges the potential barrier will gradually reduce. Experimental measurements of the maximum charge handling capacity of the pixel are reported in Section 3.

In this prototype, having six strips per pixel, the biasing scheme for the integration mode is simply obtained by means of three resistive dividers. As schematically shown in Fig. 2a each divider is connected to two strips of the pixel. When equal voltages are applied to all dividers, the drift mode is obtained (see Fig. 2b). The integration mode is obtained by changing the potential of each node of the first and the second divider by the voltages $-\Delta V_{sw}$ and ΔV_{sw} respectively, and by keeping the nodes of the third divider at a fixed potential (see Fig. 2a). Due to the fine pitch (30 μm) of the field strips the biasing circuitry must be integrated on the detector chip. The layout of the dividers and of their interconnections must be such as to avoid possible inversion of the oxide regions in both integration and drift phases. The resistors were realized with a particular p^+ implant made through an oxide layer 0.22 μm thick. This allowed to realize bonding pads over the resistive dividers in order to have access to three strips every six.

In order to minimize possible instability of the surface potential [7] that can affect detector operation, the oxide layers of the front side of the detector are covered with metal (field plate). As the voltage difference between the field strips changes from the drift to the integration phase, particular
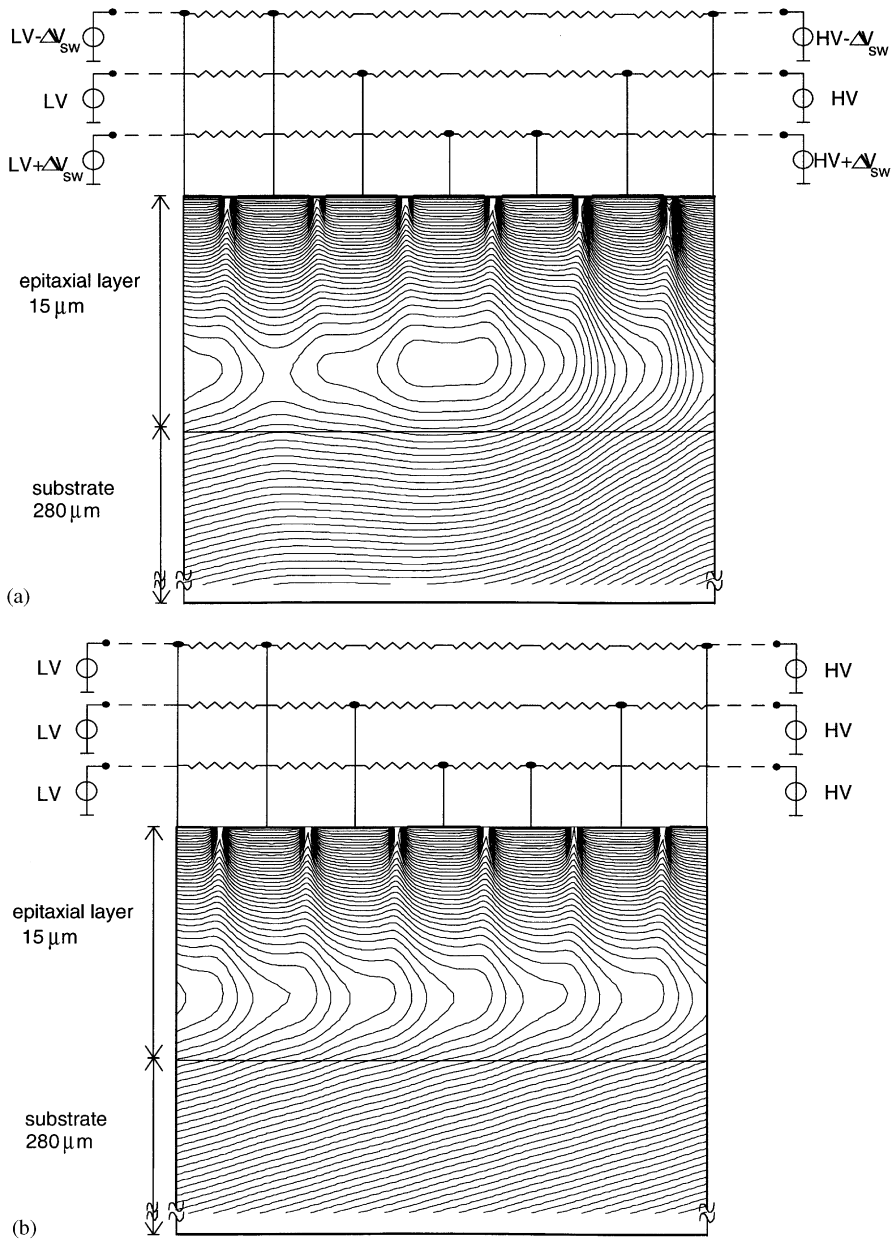
Fig. 2. Contour lines ($\Delta V = 250$ mV) of the potential distribution in a detector cross section along the drift direction in the middle of a drift channel. The biasing circuitry is also sketched. (a) Integration phase, (b) readout phase.

care has been taken in the field-plate connection. Fig. 3 shows a schematic view of the connection of the field plates within a pixel. It can be seen that in the integration phase (solid line) the voltage differ-ence between some strips is of the same polarity but higher than during the drift phase (dashed line), while the voltage difference between other strips changes sign.
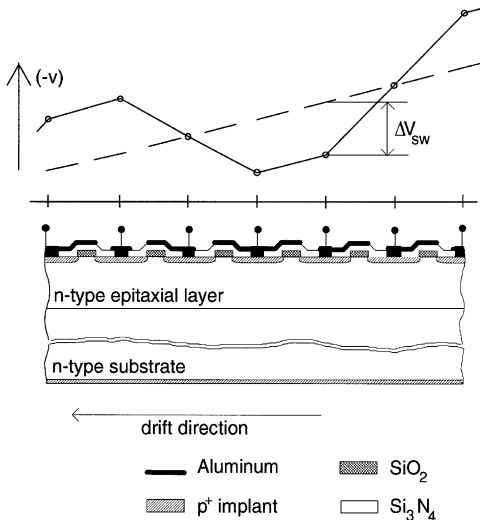
Fig. 3. Schematic view of the connection of the field plates within a pixel. The biasing scheme of the strips of a pixel during integration (solid line) and drift (dashed line) is also shown.

Fig. 4. Spectrum of ^{55}Fe measured with on-chip JFET at room temperature for a shaping time $\tau_{sh} = 250$ ns. The CDD is operated in free running. The small peak at the left of the Mn K$_\alpha$ line occurs when the X-rays are incident on the last pixel of the column (i.e. the pixel farthest from the anode). It has been verified that the distorsion of the linear drift potential near the last pixel due to side effects is responsible for partial loss of the signal charge.

Connecting the field plate placed between two contiguous p$^+$ strips to the strip at lower negative potential assures negligible hole current until the applied voltage difference exceeds the punch-through voltage. The threshold voltage of the MOS structure formed by the field plate generally puts a lower limit to the applicable voltage difference between the strips when the field plate is connected to the strip at higher negative potential.

In order to avoid spread of the signal charge to the adjacent columns (during both integration and drift), arrays of deep p-implants ("channel stops") parallel to the drift direction have been introduced [8]. The pitch of the channel-stop implants, that determines the lateral dimension of the pixel and the anode pitch, is taken equal to 180 μm (deep p-implants are 90 μm wide).

3. Experimental results and discussion

The designed prototype has been mounted and tested at room temperature. The experimental measurements aimed at testing the main operating features of the Controlled-Drift Detector.
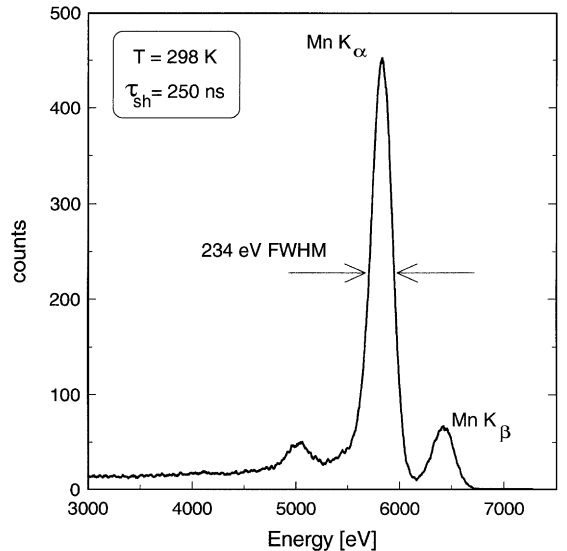
3.1. Energy resolution

Preliminary tests of the spectroscopic capability of the CDD with the on-chip electronics have been carried out. The energy resolution at room temperature was measured by operating the CDD in drift mode, that is in free run. The ^{55}Fe spectrum collected on a single readout channel (facing a sensitive area of 180 μm × 1.2 mm) with the on-chip source-follower nJFET [9] followed by external preamplification and pseudo-Gaussian shaping (shaping time $\tau_{sh} = 250$ ns) is shown in Fig. 4. The obtained energy resolution is 234 eV FWHM (corresponding to an equivalent noise charge of 24 electrons rms) for the Mn K$_\alpha$ line (5.895 keV).

3.2. Position sensing

Fast switching between the two biasing schemes is achieved by connecting external dividers of 2 μF capacitors in parallel to the first two resistive

dividers (1 node every 6) while 1nF capacitors by-pass to ground the intermediate nodes of the third resistive divider (1 node every 6). Voltage steps up to $\Delta V_{sw} = 2$ V have been tested. Of the two transitions the one from integration to readout is the more critical as the transition time must be short enough to avoid non-linearities of the transfer time from the integration minima to the collecting anode. The measured transition time for both transitions is about 26 ns (the time required for the electrons to cover a pixel length is about 50 ns at a drift field of 300 V/cm).

The integrate-drift cycle has been characterized for drift fields in the range 100–400 V/cm. A 904 nm pulsed laser with pulse duration of few nano-seconds has been focused by means of microscope optics on the front surface of the detector to gener-ate the signal charge. The laser spot diameter is about 20 μm as can be obtained by deconvolution of the experimental data from the metalization pat-tern of the field strips. The laser intensity, calibrated by [55]Fe and [57]Co sources, was adjusted to generate about 24 000 electrons, corresponding to an X-ray of about 86 keV. A shaping time of 250 ns was used for all measurements. The duration of the integra-tion phase is 360 μs.

The laser spot was positioned in the middle of a drift channel and displaced by 30 μm steps (equal to the pitch of the field strips) along the drift direc-tion. The corresponding drift time was measured. As shown in Fig. 5a, the drift time is approximately the same for any incidence point within one pixel length as the signal charge is always collected in the same integration minimum. The nearly abrupt change in the measured drift time is when the laser spot crosses the saddle point defining the border between adjacent pixels of the same column. For all experimented drift fields the non-linearity of the drift time vs. incident position is negligible com-pared to the pixel length (1% non-linearity at 300 V/cm). In Fig. 5b the same curves of Fig. 5a are shown normalized to the drift time from the last pixel. Dividing the time axis in equal time bins (dashed lines in Fig. 5b) the illuminated pixels are safely identified for all drift fields.

The measured drift times for different incidence points within the same pixel can be used to derive an average drift time per pixel. Due to the negligi-ble non-linearities mentioned above, the linear fit of the averaged drift times versus the drift coordinate of the corresponding pixel gives a good estimate of the average electron velocity (v_{av}) in the detector. In Fig. 6 the average electron velocity is plotted vs. the applied drift field. Drift velocities up to 0.5 cm/μs are achieved. The solid line represents the expected velocity $v_d = \mu_n \cdot E_d$ in a uniform drift field, where $\mu_n = 1400$ cm^2/(V s) is the electron bulk mobility. The measured electron velocity is about $0.3 \times v_d$ at 100 V/cm and $0.9 \times v_d$ at 400 V/cm. The velocity reduction is due to the residual potential perturba-tions at the depth where electron transport takes place. Two main sources of perturbation are dis-cussed here: the segmentation of the field strips and the non-linear biasing of the field strips. The seg-mentation of the field strips produces a periodic perturbation of the surface potential with a period equal to the strip pitch (= 30 μm) and an ampli-tude depending on the electrostatic properties of the silicon-oxide interface and on the strip ge-ometry. In the inset of Fig. 7 the deviations of the strip potentials from the linear fit are shown for a drift field of 300 V/cm. In addition to the inevi-table non-linearities of each divider, due to the production process, the imperfect matching of the potentials of the intermediate nodes of the three dividers introduces a periodic perturbation with a period equal to the pixel length (180 μm).

According to the Laplace equation, a sinusoidal potential perturbation $\Delta V \sin((2\pi/P_y)y)$ at one sur-face of the detector with homogeneous Dirichlet conditions at the other surface produces at a depth z a sinusoidal field having approximate amplitude $\Delta E \cong (2\pi/P_y)\Delta V \exp(-(2\pi/P_y)z)$ that reduces the average electron velocity to [10]

$$v_{av} = v_d\sqrt{1 - \beta^2} \qquad (2)$$

where $\beta = \Delta E/E_d$ is the amplitude of the field per-turbation normalized to the drift field.

As can be deduced from the simulations, the perturbation introduced by the segmentation of the field strips can be well described for our purpose as a square wave of period equal to the strip pitch and duty cycle given by the (oxide width/strip pitch) ratio (equal to $\frac{1}{6}$ in the present prototype). Expand-ing this perturbation in Fourier series and retaining
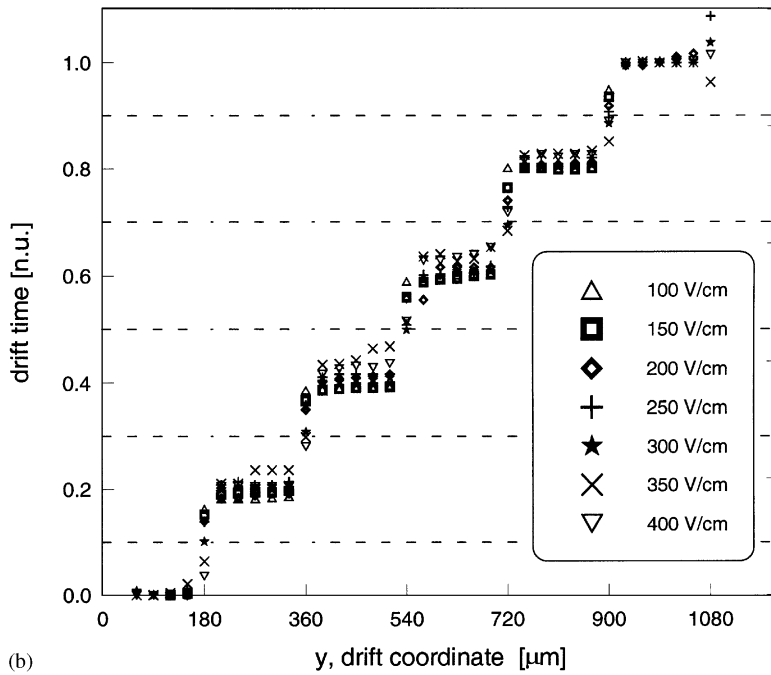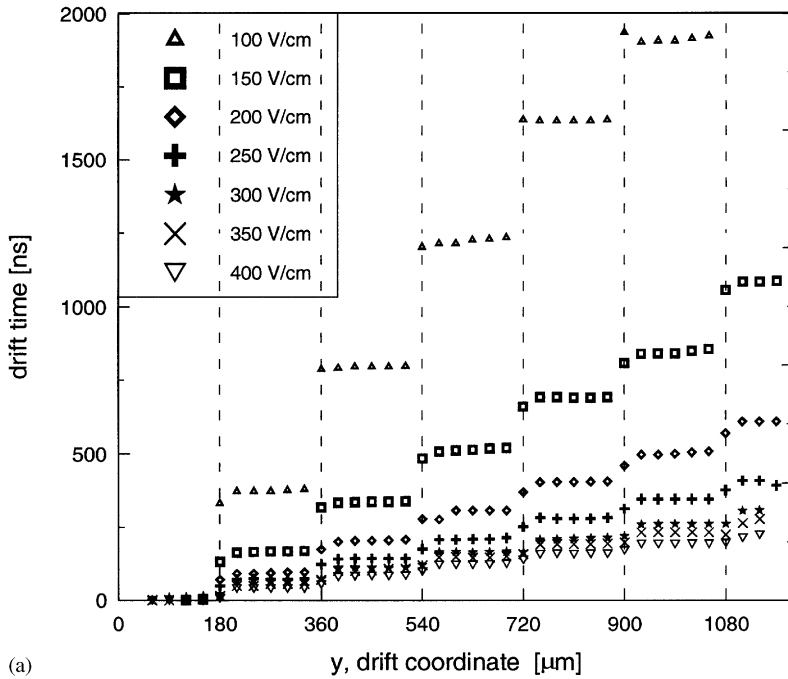
Fig. 5. Drift time vs. drift coordinate for drift fields in the range 100–400 V/cm. (a) Experimental data, (b) measured drift times are normalized to the drift time from the last pixel.
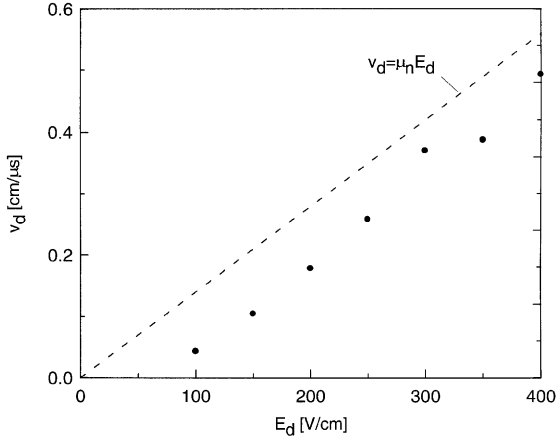
Fig. 6. Average drift velocity as a function of the applied drift field E_d. The solid line represents the nominal drift velocity $v_d = \mu_n \cdot E_d$.
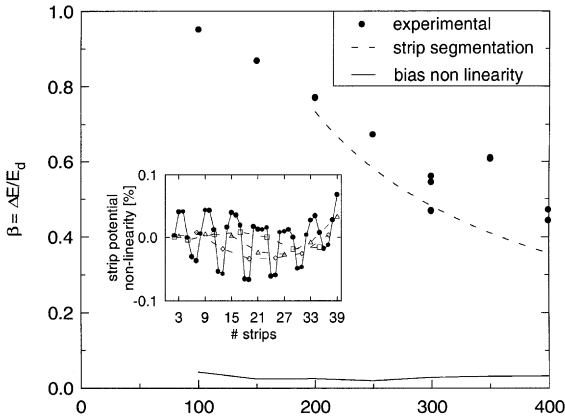

Fig. 7. Values of β as a function of the drift field. The inset shows the deviations of the strip potentials from linearity for a drift field of 300 V/cm. The light symbols ($\star$, $\square$, $\triangle$) show the intrinsic non-linearities of each divider (deviations from linear fit). The dots ($\bullet$) represent the deviations of the strip potentials from the linear fit.

only the fundamental term we obtain a good approximation of β at $z = 12\ \mu m$.

The non-linearity of the bias voltages of the field strips has been measured and can be directly Fourier-analyzed. Also in this case a pure sinusoidal wave, having a period equal to the pixel size, well approximates at $z = 12\ \mu m$ the actual effect. With these reasonable simplifications the effect of each source of perturbation on the average velocity

can be independently computed by means of Eq. (2).

In Fig. 7 the values of β are plotted as a function of the drift field. The experimental points are obtained by solving Eq. (2) for β and inserting the measured values of v_{av}. The estimated values of β due to the strip segmentation and bias non-linearities are also shown. The major contribution to β arises from the segmentation of the field strips while bias non-linearities have negligible influence on the electron velocity. Therefore it is required to cover the whole oxide surface of the active area with field plates or to use an equivalent form of passivation in order to ensure sufficient stability of the electrons' velocity.

3.3. Charge-handling capacity

A preliminary set of measurements has been carried out to characterize the charge-handling capacity of a single pixel as a function of the bias change ΔV_{sw} for the drift field of 300 V/cm. The amplitude of the potential barriers blocking the drift of the signal electrons can be tuned by varying the bias change ΔV_{sw} applied to the field strips of the front side. The signal charge was generated by an IR pulsed laser, focused on the strip above the collecting minimum of the pixel closest to the collecting anode. In this way the charge leaking from the pixel minimum is rapidly swept to the anode and the remaining charge confined within the pixel can be read by switching to the drift mode. The experimented values of ΔV_{sw} range from 1.36 V, the minimum value able to confine a small amount of electrons (equivalent to a barrier at the depth of the potential minimum of few thermal voltages) up to 2 V for which no charge leak can be observed at the maximum available laser intensity. In all the operating conditions the signal charge never leaked over the lateral barriers. The time duration of the integration phase was limited to 50 μs in order to keep the contribution of thermally generated electrons negligible.[1] In Fig. 8 the charge stored in the

---

[1] A generation rate of 1 electron/μs/pixel was measured at room temperature. Since we are dealing with high signal charges (up to 10^5 electrons) a mean value of 50 thermally generated electrons can be neglected.
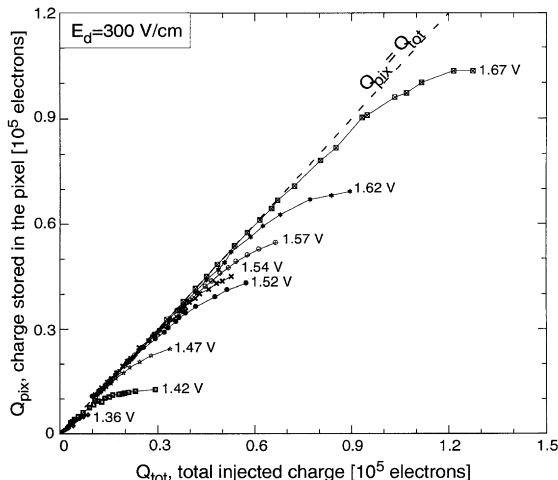
Fig. 8. Charge-handling capacity of the CDD at 300 V/cm. The charge stored in the pixel is shown as a function of the total injected charge with the bias change ΔV_{sw} as parameter.

pixel is plotted versus the total injected charge for different values of the switching signal ΔV_{sw} up to 1.67 V. When the generated charge is fully confined by the potential barriers of the pixel no output signal synchronous with the laser trigger is present and the charge stored in the pixel (proportional to the output signal measured at the anode after the transition to the drift phase) is equal to the injected charge. When the signal charge is so high to completely fill the potential well, a fraction of the injected charge leaks over the barrier in a very short time and a signal synchronous with the laser trigger appears. The fraction of the charge stored in the pixel still gives an output signal at the anode after the transition to the drift phase that tends to saturate at a maximum value. For $\Delta V_{sw} = 2$ V (not shown in Fig. 8) we could not observe any substantial leak up to the maximum laser intensity (about 10^5 electrons). Such charge handling capacity is largely sufficient for most X-ray detection applications.

3.4. Rate performance

Let us now estimate the expected rate performance of a 1 cm^2 CDD with 180 μm × 180 μm pixels. As all the pixels in a column are read out simultaneously, pulse pile-up limits the actual number of charge packets that can be stored in a column of a CDD and therefore the maximum rate. In high-resolution applications the processing time is typically greater than the drift time and therefore only one event per column is allowed. When the processing time is much shorter than the drift time more charge packets can be stored in a column, the maximum number of packets per column being eventually limited by charge broadening.

We will here restrict the analysis to the case of one charge packet (at most) stored in each pixel column (single hit). From the measured drift velocities the drift time for 1 cm distance at 300 V/cm is about $T_d = 3$ μs. The drift time also corresponds to the readout time as processing can be carried out during the integration phase.

Assuming Poisson statistics, if we require that the number of hits during the drift phase is less than 2% of the number of hits during the integration phase, we get $T_{int} = 50 \times T_d$ corresponding to a time resolution $\Delta t = (T_d + T_{int})$ of about 153 μs. In order to keep also the occurrence of multiple hits during the integration phase less than 2% of the number of single hits, the average number of single hits over 1 cm^2 active area is limited to about 2.2. The corresponding rate on the 1 cm^2 detector is about 1.4×10^4 photons/s.

References

[1] A. Castoldi, C. Guazzoni, E. Gatti, A. Longoni, P. Rehak, L. Strüder, IEEE Trans. Nucl. Sci. NS-44 (1997) 1724.

[2] A. Castoldi, C. Guazzoni, IEEE Trans. Electron Devices ED-46 (1999) 329.

[3] P. Rehak et al., Nucl. Instr. and Meth. A 248 (1986) 367.

[4] R. Hartman et al., Nucl. Instr. and Meth. A 377 (1996) 191.

[5] H. Heyns, J.G. Van Santen, IEEE J. Solid-State Circuits SC-13 (1978) 61.

[6] H. Soltau, P. Holl, J. Kemmer, S. Krisch, C.v. Zanthier, D. Hauff, R. Richter, H. Bräuninger, R. Hartmann, G. Hartner, N. Krause, N. Meidinger, E. Pfeffermann, C. Reppin, G. Schwaab, L. Strüder, J. Trümper, E. Kenziorra, J. Krämer, Nucl. Instr. and Meth. A 377 (1996) 340.

[7] A. Longoni, M. Sampietro, L. Strüder, Nucl. Instr. and Meth. A 288 (1990) 35.

[8] A. Castoldi, P. Rehak, P. Holl, Nucl. Instr. and Meth. A 377 (1996) 375.

[9] E. Pinotti et al., Nucl. Instr. and Meth. A 326 (1993) 85.

[10] A. Castoldi, P. Rehak, Rev. Sci. Instr. 66 (1995) 4989.